Proton Spin Diffusion Studies of Polymer Blends Having Modest Monomer Size. 2. Blends of Cellulose with either Poly(acrylonitrile) or Poly(4-vinylpyridine)

D. L. VanderHart,*,† R. St. John Manley,‡ and J. D. Barnes†

Polymers Division, National Institute of Standards and Technology, Gaithersburg, Maryland 20899, and Pulp and Paper Research Centre and Department of Chemistry, McGill University, 3420 University Street, Montreal, Quebec, Canada H3A 2A7

Received September 29, 1993®

ABSTRACT: Blends of cellulose (CELL) with either poly(4-vinylpyridine) (P4VPy) or poly(acrylonitrile) (PAN) have been examined by solid-state proton NMR. Multiple-pulse techniques combined with the phenomenology of spin diffusion allow one to obtain information about average domain size along the thinnest dimension of the domains. In addition, one can obtain information about the stoichiometry of the phases. CELL/P4VPy blends were examined over a composition range from 30 to 70% CELL; CELL/PAN blends spanned a composition range from 32 to 88% CELL. It was found that average overall repeat distances for the CELL/P4VPy blends were in the 8–12-nm range, while for the CELL/PAN blends the range was ca. 16–24 nm. As a function of overall composition, there were no sudden changes in dimensions or, by implication, in miscibility. As to stoichiometry, very little mixing took place; typically <5% of polymer A would be found in a polymer B-rich phase. Given this weak mixing, it is surmised that the thermodynamics of mixing are quite unfavorable for these pairs; i.e., the kinetics of phase separation are important in defining the morphology. The importance of kinetics is also manifested in a rather wide dispersion of domain size in the CELL/P4VPy blends; dispersion is smaller in the CELL/PAN blends. Small-angle X-ray scattering was also applied to a representative sample of each blend. The SAXS results corroborated the NMR results regarding domain size and size dispersion. Finally, the fact that dynamic mechanical analysis (at 11 Hz) had previously been reported on these blends enabled us to comment on the critical domain size below which the molecular motion (or T_g) for PAN would be influenced by the rigidity of the surrounding CELL phase. That critical size was found to be in the 10–13-nm range.

Introduction

In the constellation of all possible polymer blends, one is attracted to blends of cellulose with other polymers owing to the vast renewable natural sources of cellulose, its mechanical strength, and its potential for being truly biodegradable. In recognition of the manifold possibilities for hydrogen bonding in cellulose itself (five single-bonded oxygens, including three hydroxyl groups per residue), initial attempts[1-5] to make blends with cellulose focused on those polymers which could form strong hydrogen bonds. The motivating idea was that strong hydrogen bond formation should improve miscibility. (We use the term "miscible" to imply favorable thermodynamic conditions for promoting mixing on a molecular level, while terms like "intimately mixed" or "compatible" leave open the question of favorable thermodynamics.) The counterargument, for a lack of miscibility, is that it is hard for a molecule to compete with and disrupt the extensive hydrogen bonding within cellulose itself.

It is not feasible to blend cellulose in the melt with another polymer owing to the chemical instability of cellulose in the vicinity of its glass transition temperature, T_g (≈250 °C).[1] Hence, blends incorporating cellulose must be mixed in some solution form and then taken out of solution. Thus, kinetics of coagulation will be important, and, to the degree that phase separation occurs, clues about the thermodynamics of mixing of the two polymers in the absence of solvent are probably inferred more directly from the amount of molecular-level mixing (the stoichiometry of each phase) rather than the size of domains. Therefore, we undertook the present study not only because we wanted to get a reasonable estimate of domain sizes, but, more importantly, because we wanted to see whether there was mixing of cellulose chains with those of its blend partner at the molecular level.

Powerful proton NMR methods[6-9] are also now available for conducting spin diffusion experiments on polymer blends. From such experiments on phase-separated, glassy blends one can obtain information about domain size in the 3–60-nm range along with some insight into individual phase stoichiometries.

We will present spin diffusion data on two cellulose blends in this paper. The possibility that individual phases in a phase-separated morphology possess mixed composition as opposed to having pure-homopolymer composition will also be entertained. Important and useful perspectives on spin diffusion between protons on like and unlike polymeric repeat units within the *same* phase have previously been gleaned from spin diffusion data in a miscible blend; that data and interpretation were the subject of our first paper[9] in this series. The two cellulose blends we consider herein are phase-separated and consist of cellulose (CELL) mixed at varying overall compositions with either poly(acrylonitrile) (PAN) or poly(4-vinylpyridine) (P4VPy). Chemical repeat units for these polymers are included in Figures 1 and 2.

In previous studies[1,10] characterizing the CELL/PAN blends, it was concluded from dynamic mechanical studies and DSC data[1] that the CELL and PAN components were phase-separated into nearly pure phases up to ~50% CELL by weight after which the presence of CELL starts to influence the dynamic mechanical response of PAN. This was taken as evidence for the intimate mixing of PAN with cellulose at the higher cellulose contents. Subsequently, an NMR study[10] which included measurements of the longitudinal (T_1^H) and rotating frame ($T_{1\rho}^H$)

† National Institute of Standards and Technology.
‡ Pulp and Paper Research Centre and Department of Chemistry, McGill University.
® Abstract published in *Advance ACS Abstracts,* February 15, 1994.

0024-9297/94/2227-2826$04.50/0

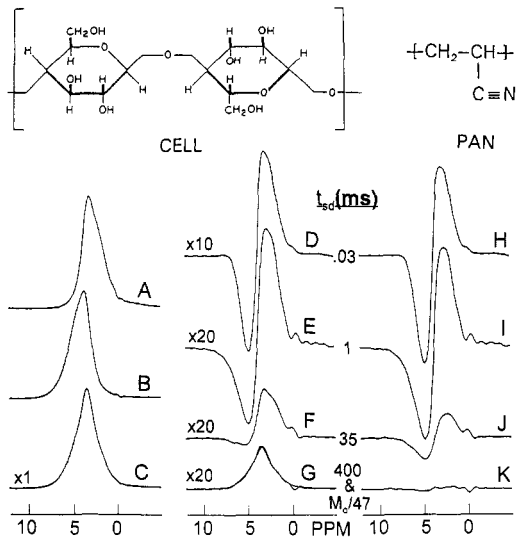

Figure 1. 200-MHz CRAMPS spectra related to spin diffusion measurements and data analysis on the 56/44 CELL/PAN blend. Normalized Boltzmann-equilibrium (M_0) spectra are pure PAN (A), pure CELL (B), and blend (C). Experimental spin diffusion spectra of the blend having total integrals of ~2% of the M_0 spectrum are given, along with vertical amplification factors referenced to C, in D–G. Corresponding spin diffusion times are 30 μs (D), 1 ms (E), 35 ms (F), and 400 ms (G). Overlaid in G is the M_0 spectrum attenuated by a factor of 47; agreement of these line shapes indicates that internal spin equilibrium has been achieved at 400 ms. Spectra H–K, associated with spectra D–G, are zero-integral spectra used for data analysis; these are linear combination spectra generated from the spin diffusion spectra and the M_0 spectrum as described in the text.

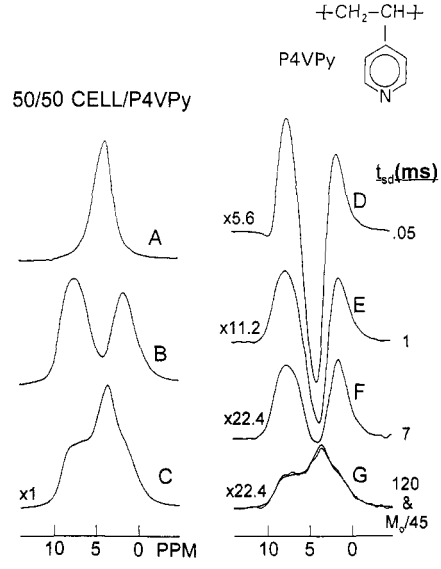

Figure 2. CRAMPS spectra, like those of Figure 1A–G, associated with the analysis of the 50/50 CELL/P4VPy blend. M_0 spectra of pure CELL (A), pure P4VPy (B), and blend (C); intensity of A is half that of B and C. Spectra D–G are spin diffusion spectra with vertical amplification factors given. Corresponding spin diffusion times are 50 μs (D), 1 ms (E), 7 ms (F), and 120 ms (G). Overlaid in G is the M_0 spectrum, attenuated by a factor of 45, of the blend showing that internal spin equilibrium has been achieved in 120 ms.

relaxation times of the protons in several of these blends concluded that there was little mixing for any proportions and that the domain sizes lay in the range from ~4 to 15 nm for a 75/25 CELL/PAN blend to ~15–35 nm for blends between 25 and 50% CELL. We sought to improve the quantitative character of these results, especially with reference to the issue of molecular-level mixing. The spin diffusion measurements reported herein offer a much more precise characterization of blend morphology than does, say, a $T_{1\rho}^{H}$ measurement, even though both rely on spin diffusion arguments. This follows from the fact that the initial polarization gradient is zero in the $T_{1\rho}^{H}$ experiment; hence one does not have the advantage of the mathematical simplicity of interpretation[11] that derives from the production of a spatially sharp, nonzero initial gradient in our spin diffusion experiments.

A previous study[5] of the CELL/P4VPy blends, which included dynamic mechanical measurements as well as ^{13}C and ^{1}H NMR measurements, concluded that the CELL and P4VPy chains are quite intimately mixed on the 2.5-nm scale over the whole composition range. This information was primarily based on the composition dependence of dynamic mechanical loss maxima and on ^{13}C NMR line shape changes which were attributed to contact between the two kinds of chains. No proton $T_{1\rho}^{H}$ arguments for mixing were invoked since the intrinsic $T_{1\rho}^{H}$ values for the homopolymers were nearly indistinguishable. Our objective was to try to clarify whether direct spin diffusion measurements supported this picture of intimate chain mixing on the 2.5-nm scale.

The fact that dynamic mechanical data are available[1,5] for these polymers will also allow us to comment on the conditions necessary for observing coupling between polymers in a blend; i.e., is coupling a result of a shrinking domain size or of the molecular-level mixing of chains?

Small-angle X-ray scattering (SAXS) was carried out on one of each of the CELL/PAN and CELL/P4VPy samples for independent comparison with the domain size information deduced from the spin diffusion data. For practical reasons the SAXS method was not applied to the other samples. Moreover, an important objective of this paper is to comment on phase stoichiometry, and this is a more difficult parameter to extract from SAXS measurements.

Experimental Section

Materials. The preparation of the CELL/PAN blends has been described elsewhere.[1] Basically, each component was dissolved in a DMAc–LiCl solution, and the solutions were combined and spread in a shallow dish. Then a coagulating agent, methanol, was gently spread over the surface of the solution, causing the formation of a gel-like material. Repeated solvent exchanges, washings, and drying yielded a solvent-free and salt-free blend. Because of the possibility of some material losses in the isolation of the dried product, the true overall stoichiometries of the CELL/PAN blends were determined by ^{13}C NMR, making the appropriate small corrections for the different cross-polarization (CP) enhancement factors for CELL and PAN. In general, the stoichiometries of the solid blends so determined indicated a preferential loss of PAN during blend preparation, based on the stoichiometries expected from the mixed solutions. Also, no evidence for CELL or PAN crystallinity was seen in the ^{13}C spectra of the blends.

The preparation of the CELL/P4VPy blends has also been described elsewhere.[5] Briefly, cellulose was dissolved in DMSO/paraformaldehyde. Dissolution involves the formation of methylol groups on the cellulose. Hence, casting a cellulose film from such a solvent results in both a partially substituted cellulose and the entrapment of some DMSO. Exposure of such cast films to a solution of 0.02 N ammonium hydroxide and subsequent drying in vacuum at 125 °C eliminate DMSO and the methylol groups. Thus, to form the blends, solutions of cellulose were mixed with P4VPy/DMSO solutions, and films were cast from this combined solution. Subsequently, the films were washed with ammonium hydroxide and dried.

All blend samples were dried for at least 24 h in vacuum at ambient temperature before the NMR experiments were run. There was no evidence of any water appearing as a narrow line in the Bloch-decay spectrum of any of these samples. The presence of protons associated with residual solvents may interfere[7] with the spin diffusion analysis; therefore, we try to

avoid having water or other residual solvents in these materials. Samples used for the spin diffusion experiments usually ranged in weight from 20 to 25 mg; the CELL/P4VPy samples ranged from 8 to 18 mg because of material availability.

Instrumentation. The experimental setup for performing the spin diffusion measurements, including the instrument, critical parameters, and pulse sequences employed, has previously been described.[7]

^{13}C spectra were collected on the CELL/PAN blends using a noncommercial spectrometer operating at 2.35 T. MAS rates were 3.2 kHz, and rf nutation frequencies were in the range 61–64 kHz. CP times were set at 1 ms, and recycle delays exceeded 5 times the T_1^H's of the protons. Weighed samples of dry PAN and dry CELL occupying identical rotor volumes were used to determine the correspondence between signal strength and weight for the determination of the true CELL/PAN stoichiometries. The cyano-carbon intensities in the PAN spectra were ignored in these determinations; only the aliphatic intensities were used.

The X-ray scattering patterns were collected on an apparatus at N.I.S.T. utilizing Cu Kα radiation and equipped with a 10-m beam path and a 2-D detector. A powder sample was placed between commercial polyimide sheets of 25-μm thickness. Cylindrical averaging about the beam direction was employed to generate the 1-D scattering patterns. Background corrections, including corrections for polyimide film scattering, were applied to obtain the scattering patterns. Lorentz corrections[12] were then applied to the scattering profile, and the intensity maximum of this corrected curve was interpreted in terms of the most probable repeat distance.

NMR Analysis Methods for Each Blend. At this point we will briefly describe the approach[7,9] used to prepare polarization gradients and analyze data for each blend. In this way, we can limit the discussion in the Results to a comparison of the PMSE-scaled data for each blend. PMSE is an acronym referring to *p*hysical *m*ixture *s*pin *e*quilibration. Spin diffusion data (which represent the departure of some measurable spectral feature from internal spin equilibrium) as a function of t_{sd}, the spin diffusion time, are scaled to a quantity called $\Delta M_s(t_{sd})$. This quantity has the property that, for any given preparation of an initial polarization gradient, $\Delta M_s(t_{sd})$ goes to unity as spin equilibration occurs within each homopolymer in the absence of any spin diffusion between protons on dissimilar chains, whereas the asymptote for $\Delta M_s(t_{sd})$ is zero when sample-wide spin equilibration is achieved. In this sense, a change of unity in $\Delta M_s(t_{sd})$ is associated with "heteropolymer spin equilibration", and that is why we will plot $\Delta M_s(t_{sd})$ over these limits. The sinusoidal period, in ppm, of initial polarization per spin imposed on the spectra is inversely proportional to n, the number of MREV-8 cycles[13] included in the polarization preparation period.

1. Cellulose/PAN Blends. Figure 1C shows M_0 CRAMPS[14] (*C*ombined *R*otation *a*nd *M*ultiple-*P*ulse *S*pectroscopy) spectra of a CELL/PAN blend whose stoichiometry as determined by ^{13}C NMR is 56/44. M_0 refers to the spectrum associated with sample-wide Boltzmann spin populations. Also shown are similar spectra for CELL (Figure 1B) and PAN (Figure 1A) homopolymer samples where the relative chemical shifts have been accurately determined by mixing each of these samples with adamantane (spectra not shown). In Figure 1D, the spin diffusion spectrum for t_{sd} = 30 μs is shown. Spectra 1E–G are similar spectra corresponding to t_{sd} = 1, 35, and 400 ms. Overlaid on the 400-ms spectrum in 1G is a scaled (by 1/47) version of the M_0 line shape, demonstrating that sample-wide spin equilibration has been achieved. Total spin diffusion integrals are all ~2% of the Boltzmann-signal integral, $I(M_0)$. Spectra 1H–K are zero-integral spectra generated from spectra 1D–G as described below and used for the spin diffusion plots.

Spin diffusion spectra were run on CELL and PAN homopolymers as well as CELL/PAN blends of the following compositions by weight as determined by solid-state ^{13}C NMR: 32/68, 35/65, 56/44, 61/39, 75/25, 82/18, and 88/12. The modest line widths of each spectrum and the significant spectral overlap of the two hompolymer spectra led to a choice of n = 52 (5 ppm sinusoidal period of the initial polarization gradient) and a rotor spinning frequency of 3000 Hz (the preparation time is 6 rotor periods). A slightly different rf frequency was then chosen for each blend to keep the spin diffusion integrals small. Spin diffusion integrals were all <2.7% $I(M_0)$ in magnitude so that line shapes would be sensitive to the progress toward spin equilibrium.[7]

The spectral overlap between CELL and PAN homopolymer spectra makes it difficult to extract the CELL or PAN contributions to the spin diffusion spectra outside of synthesizing each line shape using linear combinations of M_0 homopolymer spectra. An equally valid analysis which does not require such a line shape deconvolution for each spectrum is the following: from each spin diffusion spectrum, subtract an M_0 line shape, multiplied by $I_{tot}(t_{sd})/I_{tot}(M_0)$, where the numerator and denominator are respectively the total integrals of the spin diffusion (at t_{sd}) and M_0 spectra. This produces difference line shapes as a function of t_{sd} whose total integrals are zero but whose excursion from zero across the blend spectrum reflect the deviations from internal spin equilibrium. Following a brief spin diffusion time where homopolymer spin diffusion goes to completion, the line shape of these zero-integral difference spectra remains constant while the positive and negative peaks diminish in magnitude with increasing t_{sd}. The reason that the difference spectra have constant line shapes is that, following homopolymer equilibration at a time, say, t_{sd}', these zero-integral difference spectra (see spectra 1H–K) will all be linear combinations of undistorted homopolymer spectral contributions. Moreover, these difference spectra will have the property that the intensities associated with each homopolymer contribution are equal and opposite for all $t_{sd} > t_{sd}'$. Thus, one can monitor heteropolymer spin diffusion, i.e., the spin equilibration process between dissimilar chains, simply by measuring the relative amplitudes, $A(t_{sd})$, of these difference line shapes for $t_{sd} > t_{sd}'$. These amplitudes can then be directly related to $\Delta M_s(t_{sd})$ using the equation

$$\Delta M_s(t_{sd}) = [A(t_{sd})/A(\mathrm{PMSE})] \exp(t_{sd}/T_1^H) \qquad (1)$$

where T_1^H is the proton longitudinal relaxation time ($1.6 \le T_1^H \le 3.4$ s for the CELL/PAN blends) and A(PMSE) is the amplitude of the difference signal for the PMSE condition, i.e., after only homopolymer spin equilibration. Note that A(PMSE) is also a function of the particular choice of initial gradient. We determined the A(PMSE) values for each data set in the following way. The spin diffusion preparation, using the same n value employed for the blends, was applied to each of the homopolymer samples over a range of carrier frequencies; measurements of $I_{tot}(2\ \mathrm{ms})/I_{tot}(M_0)$ were made as a function of frequency. From these data plus a knowledge of the true stoichiometry plus the average spin diffusion total integrals for each blend data set, we calculated the initial average polarizations per spin for each homopolymer in each spin diffusion experiment. From this information we synthesized difference spectra, using linear combinations of the CELL and PAN M_0 spectra, corresponding to the PMSE condition. In this way the first term in eq 1 could be evaluated directly by ratioing these experimental and synthesized difference spectra using the Bruker-supplied software.[15] This approach assumes that the spectrum of each component in the blend is very close to that of the respective homopolymer; this assumption is borne out by the agreement between the line shapes of the experimental and synthesized difference spectra. In view of the fact that slight drifts in the experimental setup cause shifts of the apparent CRAMPS resonance frequencies, it was important that a definition of frequency, based on the position of resonances as opposed to the selection of rf frequencies, was established in the determination of A(PMSE).

2. Cellulose/Poly(4-vinylpyridine) Blends. Figure 2C shows M_0 CRAMPS spectra of a 50/50 CELL/P4VPy blend along with similar spectra for pure cellulose (2A) and pure P4VPy (2B). Also shown in Figure 2D–G are spin diffusion spectra for t_{sd} = 0.05, 1, 7, and 120 ms, respectively. The 0.05-ms spectrum approximates the initial condition. Overlaid in the 120-ms spectrum is the M_0 line shape scaled by 1/45. Total spin diffusion integrals averaged ~2.9% $I(M_0)$.

Spin diffusion spectra were run on blends with three different stoichiometries, 30/70, 50/50, and 70/30 CELL/P4VPy, as well as the pure homopolymers. Given that the intensity of the P4VPy in 3B falls into two regions, separated by ~5.7 ppm and corresponding to the aromatic and aliphatic protons, and given that the CELL resonance in 2A is found mainly between these

maxima, it makes sense that one impose an initial polarization profile whose sinusoid has a period of 5.7 ppm ($n = 46$). A proper choice of rf carrier frequency will then yield small spin diffusion integrals and initial CELL and P4VPy polarizations of opposite sign so that the spin diffusion line shapes will be sensitive to the process of spin equilibration.[7] A rotor frequency of 2831 Hz was chosen since 5 rotations corresponded to the preparation period.

Although there is significant spectral overlap between the homopolymer spectra, especially the downfield wing of the blend spectrum is dominated by the aromatic resonances of the P4VPy. Thus, while we could have analyzed these spectra using the same approach employed in the CELL/PAN blend samples, we chose rather to analyze the M_0 spectrum and each spin diffusion spectrum in each CELL/P4VPy blend utilizing this aromatic intensity. This was done by scaling the M_0 spectrum of P4VPy so that it matched the downfield wing of the spin diffusion (or the M_0 blend) spectrum and left a difference spectrum whose line shape was a scaled version of the M_0 cellulose spectrum. After the short time (≈1 ms) required for homopolymer equilibration, this method will allow one to determine the relative contributions of P4VPy and CELL to the line shapes; at shorter times; this analysis will produce somewhat distorted numbers because the aromatic and aliphatic polarizations per spin of P4VPy have not yet achieved the same level; yet, with the polarization profile chosen, the initial aromatic and aliphatic polarizations are similar so that this distortion is not great. $\Delta M_s(t_{sd})$ is then defined in terms of the parameter $R(t_{sd})$, which, in turn, is defined to be the ratio of the P4VPy aromatic spin diffusion intensity at t_{sd} relative to the intensity in the same P4VPy region in the M_0 spectrum. Thus,

$$\Delta M_s(t_{sd}) = \exp(t_{sd}/T_1^H)[(R(t_{sd}) - R')/(R(\text{PMSE}) - R')] \quad (2)$$

where $R' = I_{tot}(t_{sd})/I_{tot}(M_0)$ and R(PMSE) is the R value associated with the PMSE condition. R(PMSE) was obtained for each set of blend data from measurements of $I(t_{sd})/I(M_0)$ for pure P4VPy using the same preparation sequence and employing rf frequencies chosen to match the spectral positions of the P4VPy resonances in the corresponding M_0 spectrum of each blend.

Results

In this section we will show plots of the scaled deviation from equilibrium, $\Delta M_s(t_{sd})$, for each of the blends as a function of $t_{sd}^{1/2}$, recognizing that the interval from 1 to 0 on the ordinate is that interval which corresponds to heteropolymer spin diffusion and recognizing that such a plot, based on our computer modeling of spin equilibration, would have an initial linear portion over at least the first 65% of its decay range if only heteropolymer spin diffusion occurred and if the system had idealized (narrow distribution) lamellar or rod–matrix morphologies. The fact that homopolymer spin equilibration happens concurrently at early times with heteropolymer spin equilibration means that the former process will be interfering with respect to the latter. In our first paper in this series, we showed that, for homopolymers having monomer size and proton density similar to those encountered in this study, homopolymer spin equilibration is >99% complete afer 1 ms. Thus, to a very good approximation, for $t_{sd} > 1$ ms, $\Delta M_s(t_{sd})$ should reflect only heteropolymer spin equilibration. We shall proceed with our analysis using $\Delta M_s(t_{sd})$ data obtained for $t_{sd} \geq 1$ ms and shall interpret these data strictly in terms of heteropolymer spin equilibration.

A second perspective for these spin diffusion plots is needed because we are claiming that these kinds of experiments yield information about stoichiometries within each phase in a phase-separated morphology. Obviously, if a given phase is not a pure homopolymer phase but rather is a mixed phase, with polymers A and B mixed on a molecular scale, there will be rapid communication between the protons of polymers A and B *within the same phase*. One would argue that this intraphase heteropolymer spin equilibration should occur on a time scale very similar to homopolymer spin equilibration since distances for protons bonded to adjacent carbons are similar to distances of closest approach for protons on different molecules. Thus, one would like to separate heteropolymer spin equilibration into two parts, namely, intraphase and interphase.

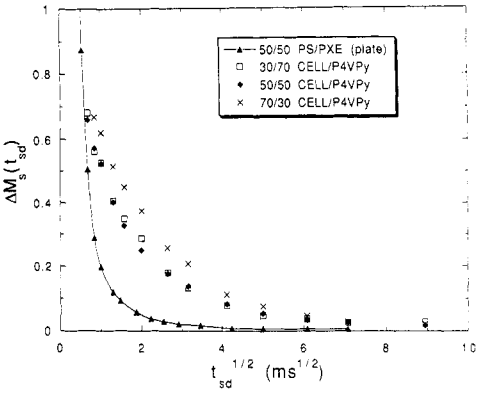

Figure 3. Scaled spin equilibration data for the three CELL/P4VPy blend samples and for the miscible 50/50 PS/PXE blend. The CELL/P4VPy blend data for times <1 ms have been deleted since homopolymer spin equilibration is dominating during this early period. Thus, these CELL/P4VPy data represent heteropolymer spin equilibration. The longer times required for spin equilibration in the CELL/P4VPy blend relative to the PS/PXE blend indicate that mixing in the CELL/P4VPy blends is spatially coarser than in PS/PXE.

To summarize the foregoing paragraph, there will be fast (and, to us, uninteresting) homopolymer spin equilibration. In addition, there *may* be intraphase heteropolymer spin equilibration which will take place on a comparably short time scale, and by capturing the amount of this short-term heteropolymer spin diffusion, one can get some indication of stoichiometries within the phases. The longest decay times will then be associated with spin diffusion between the actual domains. While one can postulate a similar time scale for homopolymer spin equilibration and intraphase heteropolymer spin equilibration, there is in the latter process an additional statistical uncertainty corresponding to the distribution of B (or A) residues near any given A (or B) residue which will lengthen the time required for intraphase heteropolymer spin equilibration relative to homopolymer spin equilibration. It is mandatory, prior to interpreting these decay curves for phase-separated blends, to appreciate what this difference in time scales is.

The polystyrene/poly(xylylene ether) (PS/PXE) blend treated in the first paper[9] in this series gives the insight we need into the process of intraphase heteropolymer spin equilibration since the PS and PXE chains are mixed on a molecular scale.[9] In that blend, this intraphase heteropolymer spin equilibration was 80% complete at t_{sd} = 1 ms. However, the final approach to spin equilibrium showed a rather long tailing; in fact, decay could still be observed in the t_{sd} = 10 ms range. Therefore, since we cannot, in general, afford to wait 10 ms before collecting data on interphase spin equilibration owing to the considerable progress of interphase equilibration over that time, we will, when an "intraphase/interphase" ambiguity arises, use the PS/PXE heteropolymer spin equilibration curve to model changes in $\Delta M_s(t_{sd})$ which are attributable to intraphase heteropolymer spin equilibration.

1. CELL/P4VPy Blends. Figure 3 shows the spin diffusion plots for the three CELL/P4VPy blends and compares these data to those of the 50/50 PS/PXE plate sample. It is clear from the longer times for equilibration

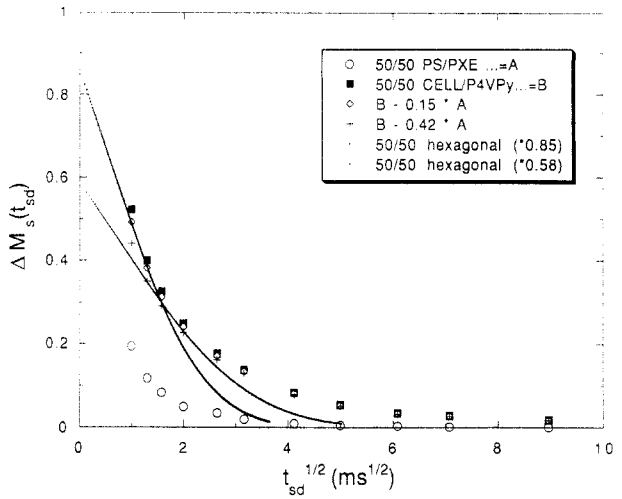

Figure 4. Two illustrative attempts to isolate the interphase from the intraphase contributions to the heteropolymer spin equilibration for the 50/50 CELL/P4VPy blend. Owing to the small domain sizes in this blend, the time scales for the intraphase and interphase equilibration are not so cleanly separable. Data "A" and "B" in the legend are respectively the experimental data for the miscible PS/PXE blend and the 50/50 CELL/P4VPy blend; the "A" data are used to model the intraphase decay rate. The difference data, "B - 0.15*A" and "B - 0.42*A", represent possible candidates for the interphase component. The two remaining densely dotted lines are theoretical interphase equilibration curves based on a hexagonal rod–matrix morphology, having ordinate intercepts dictated by the particular linear combination chosen for each set of difference data. The theoretical curve having the 0.85 intercept matches the initial slope of the corresponding difference curve; any theoretical curve having an intercept of 0.58 will not match the initial slope of its corresponding difference data. The matching of initial slopes is used as a criterion for extracting the parameters associated both with average domain size and with phase stoichiometry. The departure of the difference data, "B - 0.85*A", from the corresponding theoretical curve at longer times indicates that there is a substantial dispersion in domain size.

that the CELL/P4VPy blends are not mixed on as fine a distance scale as the PS/PXE blend is and, therefore, they are phase-separated. Making use of the PS/PXE findings, we limit data to times of 1 ms and beyond and interpret these data solely in terms of heteropolymer spin equilibration. Note that the 30/70 and 50/50 CELL/P4VPy blends have similar temporal responses while the data for the 70/30 blend extend to somewhat longer times. About one-half of the heteropolymer equilibration has occurred prior to 1 ms and this implies that domain sizes will be quite small. Since the time scales for interphase and intraphase equilibration in these samples have only modest contrast, care must be taken in analyzing these data, as will be shown.

The first step in the interpretation of the spin diffusion data is to calculate an average diffusion constant, D. This is done by calculating the proton density for both homopolymers based on their chemical formulas and their published densities[16] and assigning them D's which are proportional to the cube root of their proton densities. The calculated diffusion constant of 6.2×10^{-12} cm^2/s for alkanes[17] is used as a reference. Respectively, we calculate D's of 4.9×10^{-12} and 5.5×10^{-12} cm^2/s for P4VPy and CELL. A mean value of 5.2×10^{-12} cm^2/s was chosen as a uniform D.

Because of the smaller domains sizes, the interpretation of the heteropolymer spin equilibration curves of Figure 3, as discussed earlier, involves ambiguities with respect to the separation of the time scales for heteropolymer intraphase and interphase equilibration, assuming that phases of mixed composition exist. We choose the 50/50 blend data to illustrate Figure 4 how we attempt to separate effects arising from such intraphase and interphase processes. In an approximate sense we are asking the question whether these data are telling us, at one extreme, that phases are closer to "pure homopolymer" in composition and smaller and more varied in domain size or, at the other extreme, that phases are more mixed in composition and larger but less varied in size. We use the PS/PXE data to choose which viewpoint is more appropriate. Thus, Figure 4 reproduces the 50/50 PS/PXE data and the 50/50 CELL/P4VPy data for $t_{sd} \geq 1$ ms. In addition, hypothetical curves taking into account partial mixing in the phases are generated under the assumption that intraphase heteropolymer spin equilibration has a time dependence like that of PS/PXE. Thus the curves designated "B - 0.15*A" and "B - 0.42*A" are calculated by subtracting respectively 15% and 42% of the PS/PXE data from the CELL/P4VPy data at each t_{sd}. These difference plots then approximate remaining interphase heteropolymer equilibration assuming respectively that 15 and 42% of the heteropolymer spin equilibration represented by $\Delta M_s(t_{sd})$ arises from intraphase equilibration. The two more-continuous lines (made up of a series of closely spaced dots) in Figure 4 are theoretical decay curves corresponding to heteropolymer spin diffusion for pure-phase compositions and for idealized rod–matrix geometries. (These curves for rod–matrix morphologies are very close in shape to theoretical plots for idealized lamellar morphologies where parameters are chosen so that initial slopes match.) The larger amplitude theoretical curve in Figure 4 has a slope which matches the initial slope of "B - 0.15*A" difference data. However, these difference data decay more slowly than the theoretical curve at longer times, indicating, qualitatively, that this CELL/P4VPy blend has a substantial dispersion in domain size. The second difference curve, "B - 0.42*A", was chosen in a more arbitrary way so as to represent the idea that intraphase equilibration is more important. In other words, the motivating idea is that the curvature in the experimental data at earlier times really indicates a substantial contribution from the tailing of the intraphase equilibration. Therefore, the factor of 0.42 used in the "B - 0.42*A" data difference approximately captures the slope of the experimental data in the range of t_{sd} = 3–4 ms, and the corresponding theoretical curve in Figure 4 reproduces that slope, subject to the implied constraint that the intercept be 0.58 (=1.00 - 0.42).

The two theoretical curves of Figure 4 represent two estimates of the intraphase contribution to heteropolymer spin equilibration. We would like to choose one of these curves as being more likely to describe reality, so we introduce the criterion that a meaningful theoretical curve must at least match the initial slope of the interphase contribution to the decay. As will be discussed presently, this initial slope has the most model-independent interpretation. Yet, adoption of this criterion implies the acceptance of certain assumptions.

The two important assumptions are that (a) compositional differences at phase boundaries are step functions (no interface width) and (b) initial spin polarization differences depend strictly on composition. The first assumption is only a postulate with no further support; the implications of this assumption will be considered in the Discussion. The second assumption ought to be satisfied in our experiments. If these assumptions are valid, then the interphase spin equilibration curve plotted against $t_{sd}^{1/2}$ will exhibit the characteristic that its slope

Table 1. Model-Dependent Domain Dimensions and Stoichiometries Deduced from Spin Equilibration Curves for Three CELL/P4VPy Blends[a]

		phase stoich[b]			lamellar model		hex rod–matrix model	
composition (CELL/P4VPy)	$\Delta M_s(0)^*$	f_{mm}	f_{mj}	$t_{sd}^{1/2*}$ (ms$^{1/2}$)	L^c (nm)	$X_m{}^c$ (nm)	$L_{cc}{}^d$ (nm)	$X_d{}^d$ (nm)
30/70	0.83	0.06	0.03	2.9	9.7	2.9	10.1	5.8
50/50	0.85	0.04	0.04	2.3	7.7	3.9	10.4	7.7
70/30	0.95	0.02	0.01	3.4	11.2	3.3	11.7	6.7

[a] The uncertainty in the experimental intercepts, $\Delta M_s(0)^*$ and $t_{sd}^{1/2*}$, is estimated to be ±5% of each value. [b] Phase stoichiometries are calculated under the assumption that the mass fraction given by the overall stoichiometry stays constant when phases become mixed; e.g., in the 30/70 blend, the mass fraction of any minor phase stays at 0.30 even when phases take on a mixed composition. f_{mm} and f_{mj} are the fractions of the minor component in the minor and major phases, respectively. [c] L and X_m in the lamellar model are respectively the overall repeat distance and the domain width of the minor phase, where, for the latter, the assumption is made that the minor phase has the same mass fraction as that of the minor component of the blend. [d] In the hexagonal rod–matrix model the rods are the minor phase and have diameter X_d while L_{cc}, the center-to-center distance, is one measure of an overall repeat distance.

cannot increase in magnitude as a function of increasing $t_{sd}^{1/2}$. Therefore, if one attempts to isolate the interphase heteropolymer decay, $\Delta M_s(t_{sd})^*$, from the entire heteropolymer decay, $\Delta M_s(t_{sd})$ for $t_{sd} \geq 1$ ms, as was attempted in the curves "B – k*A" (k = 0.15, 0.42) in Figure 4, then the tangent, evaluated at t_{sd} = 1 ms, of any proposed $\Delta M_s(t_{sd})^*$, when extended back in time to t_{sd} = 0, should intersect the ordinate at a value no larger than $(1-k)$. For the family of "B – k*A" curves like those shown in Figure 4, this criterion is only fulfilled for $k \leq 0.15$. Therefore, we argue that $\Delta M_s(0)^* \geq 0.85$ for the 50/50 CELL/P4VPy blend data.

We digress to discuss the interpretation of the initial slope, S, for interphase heteropolymer spin equilibration with sharp initial polarization gradients and vanishing interface widths. S is defined by

$$S = |\partial(\Delta M_s(t_{sd})^*)/\partial(t_{sd}{}^{1/2})| \quad (3)$$

where this derivative is evaluated near $t_{sd} = 0$. S has the property that

$$S \propto WD^{1/2}[\Delta M_s(0)^*]/[f_\alpha(1-f_\alpha)] \quad (4)$$

where W is the total interfacial surface area, f_α is the fraction of total protons associated with the α phase (the two phases are designated α and β), and D is the average diffusion constant. In general, if one can extract $\Delta M_s(t_{sd})^*$ from $\Delta M_s(t_{sd})$, then S can be related directly to the interfacial surface area in a model-independent way since usually D is known and f_α is known approximately (moreover, the quantity $f_\alpha(1-f_\alpha)$ is not a strong function of f_α except when f_α approaches 0 or 1). The ambiguity in assigning morphological models to spin diffusion curves arises from the manifold ways to invent different morphologies with the same surface area. In general, the greater is the domain size dispersion at some fixed interfacial area, the earlier in time is the departure from linear behavior seen.

The conclusion regarding the 50/50 CELL/P4VPy blend data as analyzed in Figure 4 is that with $k \leq 0.15$ phase compositions are purer and domain sizes are smaller and more disperse compared to an interpretation based on, say, k = 0.42. Table 1 summarizes the parameters extracted from similar analyses, like that in Figure 4, applied to data for each of the CELL/P4VPy blends. The parameter $t_{sd}^{1/2*}$ in Table 1 is the intercept along the abscissa of each spin diffusion plot generated by a line of slope $-S$ passing through $\Delta M_s(0)^*$. The $\Delta M_s(0)^*$ $(=1-k)$ values in Table 1 are those resulting from generating a "B – k*A" curve such that its tangent at t_{sd} = 1 ms has an ordinate intercept which coincides with the value $(1-k)$. The parameters $\Delta M_s(0)^*$ and $t_{sd}^{1/2*}$ respectively yield information about stoichiometries and interfacial areas (which, in turn, are related in Table 1 to domain sizes using different morphological models).

The extraction of stoichiometric information from $\Delta M_s(0)^*$ values is an undetermined problem. One more assumption, either about the relative mass fractions or about the composition of one of the phases, is needed. In Table 1, for illustration, we adopt the assumption that the mass fraction of the phases remains the same even though the phases may be mixed. For example, in the 30/70 blend, if mixing occurs we assume that the mass fraction of the minority phase remains at 0.30. Therefore, in Table 1 we indicate the mass fractions, f_{mm} and f_{mj}, of the minior component in the minority and majority phases, respectively. As can be seen from these values in Table 1, the implied fractions are 0.06 or less. While these numbers will depend somewhat on the assumptions about mass fractions, the data suggest that the concentrations of CELL in the P4VPy-rich phases or vice versa remain small (the maximum concentration allowed would be 12% P4VPy in the CELL-rich phase in the 30/70 CELL/P4VPy blend assuming that the P4VPy-rich phase was pure).

The domain sizes in Table 1 are derived from theoretical spin diffusion curves having $t_{sd}^{1/2*}$ values which match the experimental values. This matching is, again, essentially a matching of surface areas. Thus, while the theoretical curves assume an idealized uniformity of domain sizes, the domain sizes given in Table 1 take on the meaning of a volume-fraction-averaged domain size in the context of the wide distribution of domain sizes typifying the CELL/P4VPy blends. If the 1-D lamellar model (which assumes stacks of planes of infinite extent whose alternating layer thicknesses of CELL and P4VPy add together to form the repeat distance, L) describes the blend morphology best, then these dimensions given in Table 1 will more accurately reflect the average sample dimensions. On the other hand, if the 2-D hexagonal rod–matrix morphology is more appropriate to these blends, then the rod diameter, X_d, for the minor phase and the center-to-center distance, L_{cc}, between rods provide better estimates of average dimensions. The dimensions given in Table 1 are displayed in Figure 5. The estimates of the overall repeat distances in both models fall into the range of ca. 8–12 nm; moreover, in this composition range there are no abrupt changes in overall dimensions; i.e., no significant changes in miscibility are implied.

Small-angle X-ray scattering is traditionally useful[18] for characterizing dimensions in this size range, provided a reasonable contrast in electron density exists between phases. Figure 6 shows a Lorentz-corrected scattering pattern for the 50/50 CELL/P4VPy blend. This scattering pattern is extremely broad, verifying that there is a substantial distribution of scattering lengths within this blend. The q value [$q = (4\pi/\lambda)\sin\theta$, where θ is half the scattering angle and λ is the wavelength of the radiation] of the broad scattering maximum corresponds to a repeat distance of 13.6 nm. This value is somewhat higher than

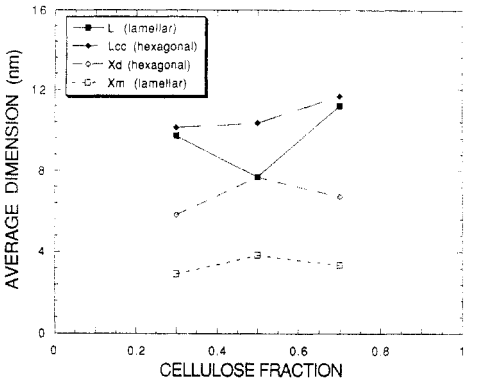

Figure 5. Plot of the average dimensions listed in Table 1 for the CELL/P4VPy blends. These data are average values deduced from the 1-D lamellar and 2-D rod–matrix morphologies. Note that there is less model-dependent fractional variation in the overall repeat distances, L and L_{cc}, compared with the variation (×2) in distance across individual domains, X_d and X_m.

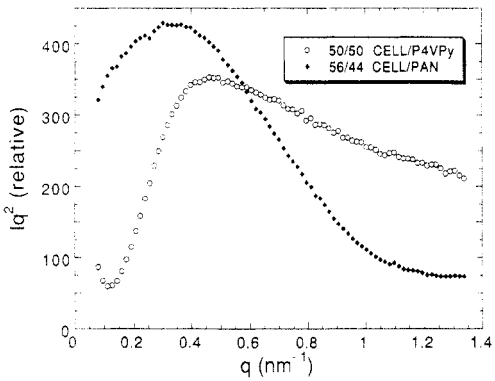

Figure 6. Lorentz-corrected SAXS scattering data for the two indicated blends. Scattering maxima correspond to repeat distances of 13.6 and 18.7 nm in the 50/50 CELL/P4VPy and 56/44 CELL/PAN blends, respectively. The strongly asymmetric shape and the long tailing of the CELL/P4VPy data toward larger q indicate a substantial dispersion of repeat distances, skewed toward sizes smaller than 13.6 nm.

the average distances (7.7–10.4 nm) deduced from the NMR data; however, we view the NMR and the SAXS data to be in agreement from the point of view that both methods indicate a wide dispersity of size and, since the SAXS data show a strong asymmetric tailing toward smaller sizes, it is very reasonable that the average scattering length in Figure 6 would be close to that seen by NMR.

The domain size and stoichiometric data taken together indicate that there is very little stoichiometric evidence for favorable thermodynamics of mixing between CELL and P4VPy, even though the domain sizes are very small, i.e., below 8 nm. Thus, we surmise that the onset of phase separation was followed very closely by the solid-state aggregation of the constituents, resulting in a kinetic entrapment of this intimate mixture. The wide dispersity of sizes also seems consistent with this view.

2. CELL/PAN Blends. Figure 7 shows data for the seven CELL/PAN blends. The characteristic decay rates for all of these blends lie in a rather narrow range, indicating that neither domain sizes nor stoichiometries are strong functions of composition. Compared with the CELL/P4VPy data of Figure 3, these decay rates are about half as fast, so characteristic dimensions will be about twice as big. Also, extrapolation of the initial slopes will be less ambiguous since the interphase heteropolymer spin equilibration process is now significantly slower than the intraphase heteropolymer spin equilibration. As a consequence, we do not bother to use the PS/PXE data to extract the interphase component; initial slopes at t_{sd} = 1 ms are just extended to t_{sd} = 0 to generate $\Delta M_s(0)^*$ values, as is illustrated in Figure 8 for the 56/44 blend.

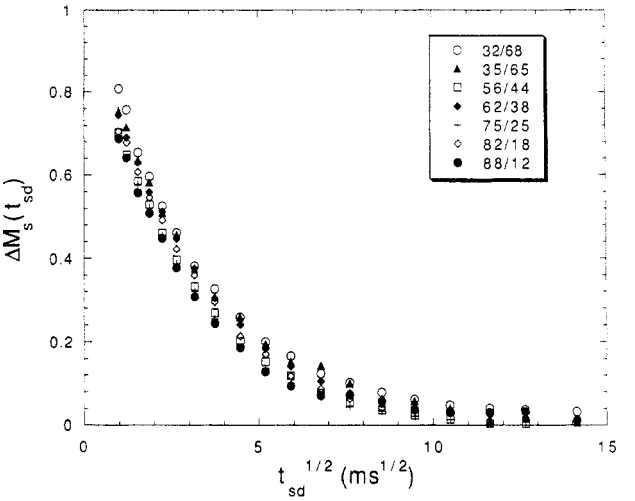

Figure 7. Heteropolymer spin equilibration curves for the indicated CELL/PAN blends. Note the uniformity of the curves, indicating a qualitative similarity of domain size and mixing within each phase.

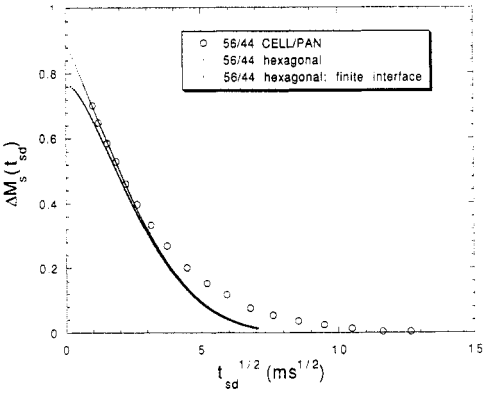

Figure 8. Comparison of the experimental heteropolymer spin equilibration data with a theoretical curve which matches the initial slope. No correction for the implied 11% intraphase contribution, using PS/PXE data, has been subtracted from the data since the time scale for interphase equilibration is sufficiently long so that the initial slope can be accurately inferred from the data. Note that the experimental data do not diverge from the theoretical curve at longer times to the same degree that divergence was seen from the 0.85-intercept curve in Figure 4. Therefore, from the NMR data, size dispersion is smaller in this CELL/PAN blend than in the CELL/P4VPy blend, a point strongly verified by the SAXS data of Figure 6. The other theoretical curve, showing early-time curvature, is an example of how a finite interface width (with a sigmoidal compositional variation across the interface) would alter the shape of the zero-interface theoretical curve assuming fixed domain size.

Table 2 summarizes the experimental parameters (the intercepts) and the deduced stoichiometric and dimensional values. The latter parameters are calculated assuming a uniform D of 5.2×10^{-12} cm²/s. Note that all the deduced values depend on the assumption that the mass fractions of the phases are identical to the mass fractions of the polymer components. This latter assumption influences L and L_{cc} primarily in the range of small minority fractions (see eq 4). X_m and X_d are more directly dependent on the validity of this assumption. The f_{mm} and f_{mj} values are also sensitive to this assumption, but when these values are small, as is the case in Table 2, then relaxing that restriction (e.g., by postulating that one of the phases is pure homopolymer in composition)

Table 2. Model-Dependent Domain Dimensions and Stoichiometries Deduced from Spin Equilibration Curves for Three CELL/PAN Blends[a]

		phase stoich[b]			lamellar model		hex rod–matrix model	
composition (CELL/PAN)	$\Delta M_s(0)^*$	f_{mm}	f_{mj}	$t_{sd}^{1/2*}$ (ms$^{1/2}$)	L^c (nm)	$X_m{}^c$ (nm)	$L_{cc}{}^d$ (nm)	$X_d{}^d$ (nm)
32/68	1.00	0.00	0.00	4.5	17.2	5.5	18.5	11.0
35/65	0.95	0.02	0.01	4.8	17.6	6.1	19.8	12.3
56/44	0.89	0.03	0.03	4.7	15.9	7.0	20.5	14.0
62/38	0.93	0.02	0.02	4.8	17.0	6.4	19.8	12.9
75/25	0.88	0.05	0.02	4.6	20.4	5.1	19.5	10.2
82/18	0.88	0.05	0.01	5.0	28.2	5.1	22.7	10.2
88/12	0.88	0.06	0.01	4.5	35.5	4.3	23.4	8.5

[a] The uncertainty in the experimental intercepts, $\Delta M_s(0)^*$ and $t_{sd}^{1/2*}$, is estimated to be ±5% of each value. [b] Phase stoichiometries are calculated under the assumption that the mass fraction given by the overall stoichiometry stays constant when phases become mixed; e.g., in a 35/65 blend, the mass fraction of any minor phase stays at 0.35 even when phases take on a mixed composition. f_{mm} and f_{mj} are the fractions of the minor component in the minor and major phases, respectively. [c] L and X_m in the lamellar model are respectively the overall repeat distance and the domain width of the minor phase, where, for the latter, the assumption is made that the minor phase has the same mass fraction as that of the minor component of the blend. [d] In the hexagonal rod–matrix model the rods are the minor phase and have diameter X_d while L_{cc}, the center-to-center distance, is one measure of an overall repeat distance.

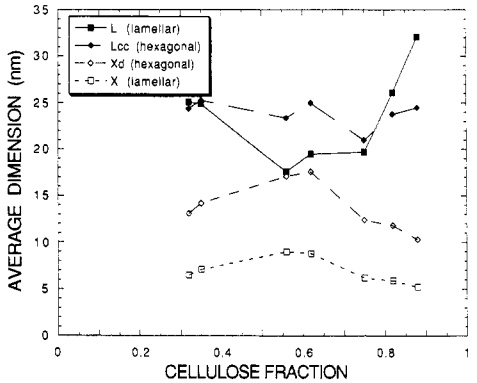

Figure 9. Plot of the average dimensions listed in Table 2 for the CELL/PAN blends. These data are average values deduced from the 1-D lamellar and 2-D rod–matrix morphologies.

limits the increase in any one of those numbers to about a factor of 2.

From the data in Table 2 and from Figures 8 and 9, the latter of which displays the deduced dimensions graphically, we arrive at the following conclusions about these CELL/PAN blends: (a) Overall repeat distances in the direction of the thinnest domain dimensions (directions of most efficient spin equilibration) are mostly in the 17–25-nm range; there is little dependence on composition. The steeper increase in L for cellulose fractions above 0.8 should probably be ignored because a minimization-of-surface-energy argument[19] would make the lamellar morphology highly unlikely over this composition range. (b) The stoichiometries of the phases indicate that there is very little mixing within the phases; hence there is very little compatibility between CELL and PAN. (c) Compared to the CELL/P4VPy blends, these CELL/PAN blends show a smaller relative dispersion of domain sizes as judged from the degree to which the data of Figures 4 and 8 depart from their corresponding theoretical curves (the larger-amplitude theoretical curve in Figure 4) at longer times. Verification of this latter point is seen clearly in Figure 6, where SAXS curves for the 56/44 CELL/PAN blend and the 50/50 CELL/P4VPy blend are compared. The CELL/PAN curve is more symmetric (with a peak corresponding to a repeat distance of ~18.7 nm); moreover, it has a significantly faster decay toward higher q, implying fewer domains having smaller dimensions. Because of the narrower dispersion of domain sizes in the CELL/PAN blends, agreement between the repeat distances determined from the peak of the SAXS curve and from the NMR analysis is expected to be much better in this CELL/PAN blend than it was in the 50/50 CELL/P4VPy blend. This expectation is borne out for the 56/44 blend in that the 18.7-nm SAXS value agrees well with the range, 15.9–20.5 nm, deduced from the NMR data.

^{13}C CPMAS spectra were taken for all of the CELL/PAN samples since there were adequate amounts for performing both proton and ^{13}C experiments. As mentioned, true CELL/PAN stoichiometries were determined this way. These spectra also verified that there was no crystallinity associated with the cellulose. No sharper features were observed in pure PAN spectra either, although this observation is less definitive for PAN spectra relative to CELL spectra since the presence of the ^{14}N nucleus may cause sufficient broadening[20,21] to mask the usual line width differences between ordered and disordered regions. Hence, for the pure PAN sample, we also tried to generate line shape changes by applying different periods of rotating frame proton relaxation prior to cross polarization. The assumption was that crystalline and disordered regions would have contrasting relaxation times and line shape contributions. This effort produced no such line shape changes; hence, we conclude that any crystallinity in PAN is very minor, if it exists at all.

These ^{13}C spectra also offered the possibility that any mixing within the phases might be detected as a departure in component line shapes from those of the pure materials. Since the proton spin diffusion results suggested very poor mixing, we did not expect to see any significant spectral changes. Our expectations were correct, with one exception, namely, the 88/12 CELL/PAN blend spectrum. In PAN, the site of strongest affinity to the hydroxyls of CELL is the nitrogen of the cyano group. Clearly, since the nitrogens are not being observed, the influence on the chemical shifts of ^{13}C nuclei due to such hydrogen bonding will be greatly diminished, albeit the cyano carbon should be the most sensitive carbon for detecting such bonding. Through a combination of fortuitous circumstances, this cyano-carbon resonance is quite sensitive to a change in the environment of the cyano nitrogen. This happens for two reasons: (a) a change in hydrogen-bonding environment will likely modify the electric field gradient surrounding the ^{14}N nucleus and (b) the 25-MHz ^{13}C line shape is quite sensitive to the orientation and magnitude of this ^{14}N electric field gradient. In Figure 10 a comparison of CPMAS spectra of pure PAN and the 88/12 CELL/PAN blend is given, using two vertical amplifications. In the lower traces, the full spectra of the PAN and blend spectra are superposed with the PAN spectrum normalized so that its aliphatic region (25–38 ppm) matches that of the blend. Above these spectra is the same comparison with an eightfold vertical amplification. There one can see that the shape of the cyano resonance in PAN (90–138

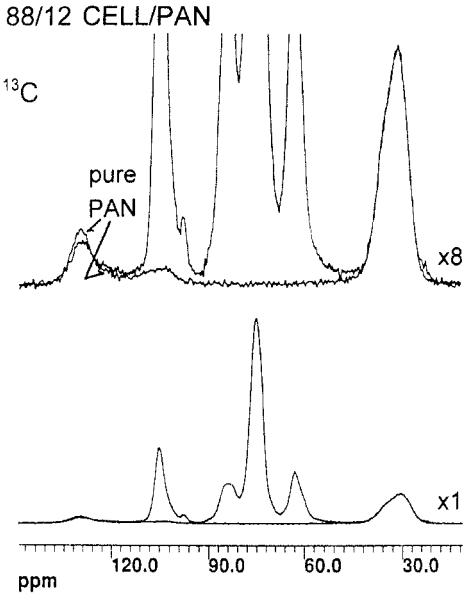

Figure 10. Comparison of 25-MHz CPMAS spectra (1-ms CP time) for pure PAN and the 88/12 CELL/PAN blend. Both spectra are overlaid in each display; the upper display has a ×8 vertical amplification. Evidence of some possible mixing is seen in the region (95–135 ppm) of the cyano carbon of the blend. Upon equalizing the intensities of the aliphatic PAN resonance (~30 ppm) in both spectra, the cyano-carbon resonance, whose shape is dictated by the nitrogen quadrupolar interaction, no longer displays the same shape. A plausible reason for the shape change is a modification of the nitrogen electric field gradient as a result of interaction with CELL. This shape change is not due to rf mismatch during CP.

ppm) consists of two broad maxima separated by ~25 ppm. This doublet arises from an unaveraged dipolar interaction between the ^{13}C and ^{14}N nuclei,[20,21] owing to the fact that the latter nucleus is not fully quantized along the static magnetic field. The ^{14}N nucleus in a cyano group has a substantial quadrupolar coupling to the electric field gradient, and this interaction competes with the Zeeman interaction in determining the quantization axis. If the electric field gradient changes, this cyano-carbon line shape will also change. Figure 10 captures some evidence for such changes. By normalizing the intensities of the aliphatic resonances in pure PAN to that of PAN in the 88/12 blend, one would also expect the cyano-carbon resonances to superpose if there were no mixing. However, what is observed is that the cyano-carbon resonance in the blend, relative to pure PAN, is depressed by ~16% in the region of the peak near 129 ppm and is enhanced in the region from ~116 to 124 ppm; this indicates that a fraction of perhaps 0.16 of the PAN residues is in an environment different from that of pure PAN. No other blend showed this change, and we ascribe this observation in the 88/12 blend to (a) the very weak trend in Table 2 toward more mixing at the lower PAN contents and (b) the greater fraction of PAN residues which exist at interfaces as the fraction of PAN diminishes.

Discussion

The cellulose blends which have been studied in this paper have been formed by processes which deal, in one way or another, with the limited solubility of cellulose and its strong tendencies to self-associate and solidify. Therefore, it is not surprising that kinetics of aggregation as well as thermodynamics might play a role in the determination of the resulting morphologies. In some respects it is gratifying that these blends are mixed on such a fine scale, i.e., with average minimum domain dimensions in the 3–15-nm range. Certainly, mixing on a scale this small implies that the physical properties of the blends will take on some intermediate character with respect to the corresponding properties of the components. However, from the points of view of both long-term and morphological stability and materials manufacture, it is important to know whether the constituents of the blend are far from thermodynamic compatibility; i.e., they wish to phase-separate into phases of relatively pure-homopolymer composition.[22] If the latter is true, as it seems to be in these materials, then one can anticipate a potentially strong dependence of morphology on the kinetics of the aggregation process. Moreover, if one wishes to maintain the morphology formed, one must avoid exposing the samples to conditions where molecular mobility might generate further phase separation.

The idea is probably correct that it will take a polymer with strong hydrogen-bonding characteristics to blend with cellulose. However, cellulose forms many hydrogen bonds with itself, and one must be able to overcome these to promote blending. Perhaps P4VPy and PAN with their single sites of hydrogen-bonding affinity per residue could not compete with the strong cellulose–cellulose interactions. Although PAN is closer to cellulose than is P4VPy in the number of sites of affinity per heavy atom (carbon, nitrogen, oxygen), the stoichiometries of the phases, as determined in this study, did not indicate that PAN was superior to P4VPy in its ability to form a mixed phase with CELL. The fact that the domain sizes in the CELL/P4VPy blends are smaller than in the CELL/PAN blends is most likely a result of combined kinetic and thermodynamic considerations rather than an indication that P4VPy is more thermodynamically compatible than PAN with CELL.

Recall that in the analysis of the CELL/P4VPy spin diffusion data we took advantage of the fact that interphase spin equilibration curves were typified by slopes which, if anything, decreased in magnitude as $t_{sd}^{1/2}$ increased. On this basis we argued that the early curvature in the spin diffusion data indicated a wider dispersion in domain size rather than more extensive mixing within the phases. This analysis was based on the assumption of negligible interface width, and we now comment on a few characteristics of theoretical spin equilibration curves for finite interfaces. Also, we state how the assumption of finite interfaces influences conclusions about stoichiometry and average domain size.

A finite interface over which composition changes continuously causes the interphase spin equilibration curves to be modified in the following way. Principal departures from the zero-interface-width curve (with constant overall phase dimensions) occur at short times. As one moves along the linear region of such a zero-interface curve (see, for example, the theoretical curves of Figure 4), toward shorter times, the curve appropriate to the finite interface bends over, instead of remaining linear, with a slope of decreasing magnitude as one approaches the $t_{sd}^{1/2} = 0$ intercept. It is also true of these finite-interface curves that, for a fixed domain size, their maximum slopes never quite achieve the maximum slopes which the corresponding zero-interface curves attain. The analysis used in Figure 4 applied the criterion that a meaningful (and zero-interface-width) theoretical curve should match the initial slope of any proposed interphase spin equilibration curve. One can use the foregoing qualitative characteristics of the finite-interface curves to predict how finite interfaces would influence the parameters deduced from such a matching of initial slopes. Qualitatively, the effects are

to *overestimate* both the average domain dimensions and the amount of mixing which exists in the interior of each phase. In other words, invoking finite interfaces in these CELL blends moves the actual stoichiometry associated with the interior regions of each phase in the direction of purer composition relative to the numbers in Tables 1 and 2. This implies even less favorable thermodynamics of mixing.

X-ray scattering curves may offer some insight into the question of finite interfaces via so-called Porod plots where theory predicts[23] that when interfaces are sharp, the intensity should vary as q^{-4} at larger q values. If we look for a power-law dependence for the scattering intensity in the larger q range, using the data presented in Figure 6 (Porod plot not shown), then for the CELL/P4VPy blend the intensity varies uniformly as $q^{-2.6}$ over the range $0.6 < q < 1.3\ nm^{-1}$. In contrast, for the CELL/PAN blend the intensity has an *average* dependence much closer to q^{-4}, although the dependence changes continuously from about q^{-5} to q^{-3} over this same range of q. In the CELL/P4VPy blend were are not convinced that contributions to the scattering at the larger angles are dictated only by the interface characteristics, owing to the strong dispersion of domain sizes. Therefore, we will not use the X-ray data to argue about interface characteristics in the CELL/P4VPy blend. For the CELL/PAN blend, which has a smaller dispersion of domain size, the qualitative indication from the "average" q dependence is that interfaces are quite sharp; nevertheless, we withhold firm judgment on this matter since the variation in the q dependence is not understood.

Earlier studies have reported dynamic mechanical analysis (DMA) measurements at 11 Hz of tan δ and the loss of storage moduli for several of the CELL/P4VPy[5] and CELL/PAN[1] blends. These results together with the NMR data on the same materials allow us to comment on the relationship between domain size and DMA observations of coupling between blend constituents. In the CELL/P4VPy system, the loss-peak temperature associated with the T_g of P4VPy changed as a function of blend composition over the whole compositional range. In contrast, the loss-peak temperature associated with the PAN T_g in CELL/PAN blends shifts with composition only over the cellulose-rich compositional range. In view of the compositional purity of the phases as seen in these NMR experiments, we can surmise that the variation in loss-peak temperature with composition in these blends arises principally from the small average dimension associated with the P4VPy- or PAN-rich phase of the blends. Moreover, we can refer to the X_m and X_d data of Tables 1 and 2 to estimate the domain size below which the mechanical response of one polymer is influenced by the presence of another polymer. The CELL/PAN data are more definitive than the CELL/P4VPy data in this regard since the published DMA data as a function of composition show the *onset* of peak-loss-temperature sensitivity at a composition of ca. 50/50, which composition turns out to be 62/38 by the ^{13}C analysis. From Table 2, the X_d value for the 62/38 CELL/PAN blend is ~13 nm; moreover, other X_d values associated with blends of larger CELL fraction have smaller X_d's corresponding to the PAN-rich phase. Therefore, we expect that DMA measurements at 11 Hz will show a coupling to the surrounding phase when the minimum dimension of that phase falls below ~10–13 nm. A similar and analogous characteristic domain size of 15 nm has been associated with DMA measurements at 110 Hz using electron microscopy data to measure domain size.[24] Since we do not know whether the morphology of the CELL/PAN blends resembles more closely the hexagonal rod–matrix or lamellar morphology, we favor the rod–matrix model to deduce this critical dimension for DMA coupling. Given that the X_m values are always half the X_d values, we defend the use of the X_d values over the X_m values because, especially at the higher CELL contents, the rod–matrix morphology would be preferred for minimizing interfacial energies.[19]

Finally, these studies have shown that X-ray scattering data and NMR spin diffusion data should be considered complementary in the sense that the estimates of domain size and the qualitative indications of the dispersion of size are in reasonable agreement. The criteria for testing for spatially sharp interfaces are probably easier to apply using the scattering data. On the other hand, this study underscores the utility of the NMR method for obtaining information about the stoichiometry of the phases.

Conclusions

Solid-state proton spin diffusion measurements of several blends of cellulose (CELL) with either poly(acrylonitrile) (PAN) or poly(4-vinylpyridne) (P4VPy) have enabled us to characterize average domain sizes (along the directions of the thinnest dimensions). It is also shown by relating these analyses to SAXS scattering data on two representative blends that the NMR-determined domain sizes are in good agreement with more conventional SAXS measures of domain size. Moreover, the SAXS data also support the claim that the NMR data are sensitive to the relative amount of domain-size dispersion. Most importantly, as a motivation for applying this NMR method (in addition to the SAXS method) to the characterization of blends, we have shown that one can obtain important information about phase stoichiometry. The latter information carries what we feel is valuable information about the thermodynamic compatibility of the blend constituents.

The average repeat distances along the thinnest morphological dimension were about twice as big (≈20 nm) in the CELL/PAN blends compared with the CELL/P4VPy blends (≈10 nm). The stoichiometry of the phases tended toward pure homopolymer; i.e., <12% of polymer A exists in the polymer-B-rich phase and, more typically, <5%. Moreover, there were no regions of composition associated with abrupt changes in morphology or stoichiometry. ^{13}C analysis in the CELL/PAN blends also showed a lack of direct spectral evidence for mixing except for the 88/12 CELL/PAN blend where perhaps as many as 16% of the PAN residues might be associated with cellulose. The lack of mixing in the phases is taken to indicate a very unfavorable thermodynamics of mixing, in spite of the strong hydrogen-bonding capability of each blend constituent. It is conceivable that one cannot easily overcome the strong tendency for CELL to hydrogen bond with itself. Nevertheless, it should not be overlooked that a very intimate level of mixing has been achieved in these blends, in spite of their thermodynamic incompatibility. Moreover, from a dynamic mechanical point of view, many of these samples show that the dynamic behavior of the noncellulosic component has been modified by blending; hence, one might expect that blending has achieved a fine enough scale such that intermediate mechanical properties will be exhibited. Since the fine scale of blending must be strongly influenced by the kinetics of solid-state aggregation, it is likely that refinements in processing would result in increased control of the resulting morphology, including the realization of even more intimate mixing.

References and Notes

(1) Nishio, Y.; Roy, S. K.; Manley, R. St. J. *Polymer* **1987**, *28*, 1385.
(2) Nishio, Y.; Manley, R. St. J. *Macromolecules* **1988**, *21*, 1270.
(3) Nishio, Y.; Manley, R. St. J. *J. Polym. Sci. Eng.* **1990**, *30*, 71.
(4) Masson, J.-F.; Manley, R. St. J. *Macromolecules* **1991**, *24*, 6670.
(5) Masson, J.-F.; Manley, R. St. J. *Macromolecules* **1991**, *24*, 5914.
(6) Caravatti, P.; Neuenschwander, P.; Ernst, R. R. *Macromolecules* **1985**, *18*, 119.
(7) Campbell, G. C.; VanderHart, D. L. *J. Magn. Reson.* **1992**, *96*, 69.
(8) Caravatti, P.; Neuenschwander, P.; Ernst, R. R. *Macromolecules* **1986**, *19*, 1895.
(9) VanderHart, D. L. *Macromolecules*, in press.
(10) Masson J.-F.; Manley, R. St. J. *Macromolecules* **1992**, *25*, 589.
(11) Crank, J. *The Mathematics of Diffusion*; Oxford University Press: London, 1957.
(12) Klug, H. P.; Alexander, L. E. *X-ray Diffraction Procedures*; Wiley: New York, 1954; Chapter 3.
(13) Rhim, W.-K.; Elleman, D. D.; Vaughan, R. W. *J. Chem. Phys.* **1973**, *59*, 3740.
(14) Ryan, L. M.; Taylor, R. E.; Paff, A. J.; Gerstein, B. C. *J. Chem. Phys.* **1980**, *72*, 508.
(15) Certain commercial companies are named in order to specify adequately the experimental procedure. This in no way implies endorsement or recommendation by NIST.
(16) *Polymer Handbook*, 3rd ed.; Brandrup, J., Immergut, E. H., Eds.; Wiley: New York, 1989.
(17) Douglass, D. C.; Jones, G. P. *J. Chem. Phys.* **1966**, *45*, 956.
(18) Porod, G. In *Small Angle X-ray Scattering*; Glatter, O., Kratky, O., Eds.; Academic Press: London, 1982; Chapter 2.
(19) Molau, G. E. In *Block Copolymers*; Aggarwal, S. L., Ed.; Plenum: New York, 1970; pp 79–106.
(20) VanderHart, D. L.; Gutowsky, H. S.; Farrar, T. C. *J. Am. Chem. Soc.* **1967**, *89*, 5056.
(21) Naito, A.; Ganapathy, S.; McDowell, C. A. *J. Chem. Phys.* **1981**, *74*, 5393.
(22) Krause, S. In *Polymer Blends*; Paul, D. R., Newman, S., Eds.; Academic Press: New York, 1978; Vol. 1, Chapter 2.
(23) Porod, G. *Kolloid Z. Z. Polymer* **1952**, *125*, 51–57, 108–122.
(24) Kaplan, D. S. *J. Appl. Polym. Sci.* **1976**, *20*, 2615.